Physical limits to chemical sensing by cells and cell populations

Andrew Mugler*

1 Introduction

Cells are amazing sensors. Rod cells in our visual system can detect single photons [1], olfactory cells [2] and immune cells [3] can detect single molecules, and amoebae can respond to a difference of about ten molecules between their front and back [4]. It makes sense for cells to be so good at this task, because successful function relies on precise detection of signals in their environment. Plus, cells have had a long time to evolve excellent biological mechanisms for sensing. Are cells "done" evolving in this realm? Have they reached the limit?

To answer this question, one might think it necessary to investigate the sensory mechanisms of individual cell types in great biological detail. However, it turns out that the the fundamental limits to sensory precision are ultimately set by the basic physics of the environment and the sensory process itself, not the specific biological details of the cell. After all, if cells truly do operate near the fundamental limits of sensory precision, then at some point they are battling physics, not biology.

In these lectures I will review the physical limits to cellular sensing, including some of the main approaches, techniques, insights, and applications to experiments. I will take a historical approach, starting with pioneering work on chemical sensing by single cells, and extending to modern-day results on collective sensing by cell populations.

2 Limits to single-cell sensing

The physics of cellular sensing was first studied more than 40 years ago by Howard Berg and Edward Purcell in the context of detecting a uniform chemical concentration [5]. Berg and Purcell reasoned that no matter what the biological sensory mechanism is, the cell will essentially act like a device that counts molecules entering its vicinity (**Fig. 1**). They began with a simple scaling argument for how the precision of sensing should depend on the properties of the concentration and the cell.

*Department of Physics and Astronomy, Purdue University, amugler@purdue.edu

If the chemical concentration is c_0, and the cell has a lengthscale a, then the average number of molecules within the cell's volume should scale like $\bar{n} \sim c_0 a^3$. Because the concentration molecules are subject to diffusion, there will be fluctuations around this average, and the precision can be characterized by the standard deviation relative to the average itself, $\epsilon \equiv \sigma/\bar{n}$. Diffusion is a Poisson process, meaning that the number of molecules within any volume is Poisson distributed, and for a Poisson distribution the variance equals the mean, $\sigma^2 = \bar{n} \sim c_0 a^3$.

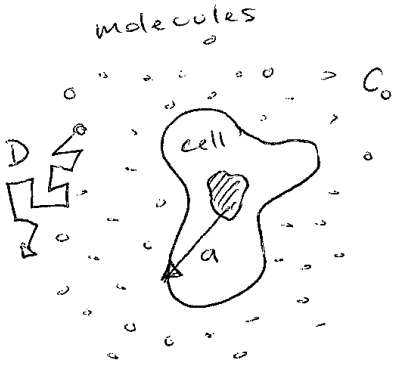

Figure 1: Concentration sensing.

However, Berg and Purcell reasoned that the cell could reduce this variance if it made multiple measurements of the molecule number, so long as there is enough time between measurements to ensure that they are statistically independent. This timescale is given by a^2/D, the approximate time for a molecule with diffusion coefficient D to diffuse out of the cell volume. Therefore, in a total time T, the cell would make $T/(a^2/D) = DT/a^2$ independent measurements, reducing the variance to $\sigma_T^2 \sim c_0 a^3/(DT/a^2) = c_0 a^5/DT$. The ratio ϵ, the square of which we will call the relative error, then scales like

$$\epsilon^2 \equiv \frac{\sigma_T^2}{\bar{n}^2} \sim \frac{c_0 a^5}{DT} \frac{1}{(c_0 a^3)^2} = \frac{1}{a T c_0 D}. \tag{1}$$

We see that sensory precision increases if the cell is larger or measures for a longer time, or if the molecules are more concentrated or diffuse faster.

As we will see, specific models of sensing give various numerical prefactors or additional terms, but the scaling is always as in Eq. 1.

2.1 The perfect sink

The first specific model considered by Berg and Purcell is a spherical cell of radius a that perfectly absorbs all molecules that contact its surface (a perfect sink, **Fig. 2**). The concentration $c(\vec{x}, t)$ obeys the diffusion equation

$$\dot{c} = D\nabla^2 c. \tag{2}$$

In steady state, and with spherical symmetry, the diffusion equation becomes

$$0 = D r^{-2} \partial_r (r^2 \partial_r c), \tag{3}$$

which is solved by

$$c(r) = -\frac{A}{r} + B \tag{4}$$

for some constants A and B. Perfect absorption at the surface and a constant concentration c_0 at infinity imply the boundary conditions $c(a) = 0$ and $c(\infty) = c_0$, respectively, which determine A and B, giving

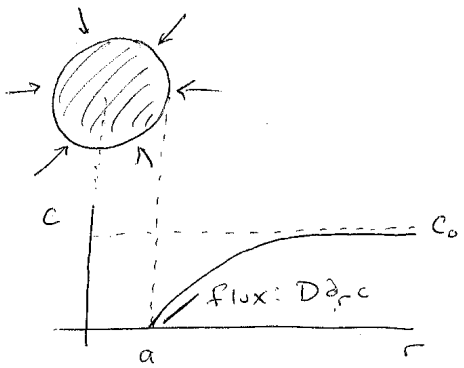

Figure 2: The perfect sink.

$$c(r) = c_0 \left(1 - \frac{a}{r}\right). \tag{5}$$

The inward flux of molecules per area per time at any radius r is given by $D\partial_r c$. Therefore, the total flux of molecules per time at the cell surface is

$$J = 4\pi a^2 \times D\partial_r c|_a = 4\pi a D c_0. \tag{6}$$

In a time T, the cell absorbs

$$\bar{M} = 4\pi a D c_0 T \tag{7}$$

molecules.

Of course, this number $\bar{M}$ is an average, because the diffusion equation is a field equation that does not account for the particulate nature of the molecules. However, under the assumption that each molecule is independent from the others, we know that the statistics of M are Poissonian. Therefore, the variance equals the mean, and the relative error is [6]

$$\epsilon^2 = \frac{\sigma_M^2}{\bar{M}^2} = \frac{1}{\bar{M}} = \frac{1}{4\pi}\frac{1}{aTc_0D}. \tag{8}$$

The perfect sink recovers the scaling of Eq. 1 with a numerical prefactor of $1/4\pi$.

2.2 The "perfect instrument"

The second model considered by Berg and Purcell is a spherical cell that is permeable to the molecules and counts the number of molecules inside its volume (**Fig. 3**, top). Berg and Purcell called this model the "perfect instrument" and derived its relative error using the autocorrelation function [5]. Here we will derive the same result using an alternative approach, Langevin dynamics, because it is easier to extend this approach to multicellular problems later.

Figure 3: The perfect instrument.

The perfect instrument imposes no boundaries because it is permeable to the molecules. Therefore the steady-state solution to the diffusion equation (Eq. 2) is $c(\vec{x},t) = c_0$. There are equal fluxes of molecules in and out of the cell, and therefore we cannot investigate the precision using the net flux as above. How do we find the relative error?

The approach we use here is to endow the diffusion equation with a Langevin noise term that accounts for the particulate nature of the molecules,

$$\dot{c} = D\nabla^2 c + \eta. \tag{9}$$

Here $\eta(\vec{x},t)$ produces the molecular fluctuations, and we will give its statistical properties later on. The consequence is that c now acquires spatiotemporal fluctuations on top of the uniform background c_0 (**Fig. 3**, bottom),

$$c(\vec{x},t) = c_0 + \delta c(\vec{x},t). \tag{10}$$

Our goal is to calculate how the fluctuations in c translate to fluctuations in the number of molecules n in the cell volume V,

$$n(t) = \int_V d^3x\ c(\vec{x},t), \tag{11}$$

or more specifically to

$$n_T = \frac{1}{T}\int_0^T dt\ n(t), \tag{12}$$

which is the average of n over a time T.

The mean of n_T is clearly the same as that of n,

$$\bar{n} = c_0 V = \frac{4}{3}\pi c_0 a^3. \tag{13}$$

To find the variance of n_T, we calculate the power spectrum of $n(t)$,

$$S_n(\omega) = \int \frac{d\omega'}{2\pi} \left\langle \tilde{\delta n}^*(\omega')\tilde{\delta n}(\omega) \right\rangle, \tag{14}$$

where $\tilde{\delta n}(\omega)$ is the Fourier transform of the fluctuations in n,

$$\tilde{\delta n}(\omega) = \int dt\ \delta n(t) e^{i\omega t} = \int_V d^3x \int \frac{d^3k}{(2\pi)^3}\ \tilde{\delta c}(\vec{k},\omega) e^{-i\vec{k}\cdot\vec{x}}. \tag{15}$$

The second step follows from Eq. 11 and the properties of the Fourier transform (see Appendix A). As long as the cell's integration time is much longer than the typical diffusion timescale, $T \gg a^2/D$, the variance of n_T is given by the low-frequency limit of the power spectrum,

$$\sigma_T^2 = \frac{1}{T} S_n(\omega \to 0). \tag{16}$$

Eq. 16 follows from the fact that the power spectrum is the Fourier transform of the autocorrelation function and is proven in Appendix B.

To find the power spectrum $S_n(\omega)$, we insert Eq. 10 into Eq. 9,

$$\dot{\delta c} = D\nabla^2 \delta c + \eta, \tag{17}$$

Fourier transform it,

$$-i\omega\tilde{\delta c} = -Dk^2\tilde{\delta c} + \tilde{\eta}, \tag{18}$$

and solve for $\tilde{\delta c}$,

$$\tilde{\delta c} = \frac{\tilde{\eta}}{Dk^2 - i\omega}. \tag{19}$$

We insert Eq. 19 into Eq. 15 and the result into Eq. 14,

$$S_n(\omega) = \int_V d^3x d^3x' \int \frac{d\omega'}{2\pi} \frac{d^3k}{(2\pi)^3} \frac{d^3k'}{(2\pi)^3}\ \frac{e^{-i\vec{k}\cdot\vec{x}} e^{i\vec{k}'\cdot\vec{x}'}}{(Dk - i\omega)(Dk' + i\omega)} \left\langle \tilde{\eta}^*(\vec{k}',\omega')\tilde{\eta}(\vec{k},\omega) \right\rangle. \tag{20}$$

Now we need the statistics of η, which are given by

$$\langle \eta(\vec{x}',t')\eta(\vec{x},t)\rangle = 2Dc_0\delta(t-t')\vec{\nabla}_x \cdot \vec{\nabla}_{x'}\delta(\vec{x}-\vec{x}'). \tag{21}$$

Eq. 21 can be derived by approximating diffusion as a discrete hopping process on a 3D lattice and taking the continuum limit [7]. The hopping reactions are delta-correlated in time, but they are anti-correlated in space because the loss of a molecule at one lattice site produces a gain of one molecule at a neighboring site; these spatial correlations lead to the gradients in Eq. 21. In Fourier space, Eq. 21 reads

$$\left\langle \tilde{\eta}^*(\vec{k}',\omega')\tilde{\eta}(\vec{k},\omega) \right\rangle = 2Dc_0 \times 2\pi\delta(\omega-\omega') \times k^2(2\pi)^3\delta(\vec{k}-\vec{k}'). \tag{22}$$

Inserting Eq. 22 into Eq. 20, the low-frequency limit of the power spectrum becomes

$$S_n(0) = \frac{2c_0}{D} \int_V d^3x d^3x' \int \frac{d^3k}{(2\pi)^3}\ \frac{e^{-i\vec{k}\cdot(\vec{x}-\vec{x}')}}{k^2}. \tag{23}$$

These integrals are straightforward and are performed in Appendix A. The result is

$$S_n(0) = \frac{16\pi c_0 a^5}{15D}. \tag{24}$$

Therefore, using Eqs. 13 and 16, the relative error is

$$\epsilon^2 = \frac{\sigma_T^2}{\bar{n}^2} = \frac{3}{5\pi}\frac{1}{aTcD}. \tag{25}$$

This is the same result obtained by Berg and Purcell [5]. The perfect instrument recovers the scaling of Eq. 1 with a numerical prefactor of $3/5\pi$. The precision of the perfect instrument is $(3/5\pi)/(1/4\pi) = 2.4$ times worse than that of the perfect sink (Eq. 8) because the sink does not count any molecule more than once [6].

2.3 Including binding kinetics

Over the past 40 years, the above models have been extended to include features that more realistically reflect cell biology. One of the most important features is that cells detect molecules using receptors on their surface, and if a receptor is already bound it cannot detect a second molecule (**Fig. 4**). The receptor must either release the molecule or be internalized by the cell and replaced by another receptor. Berg and Purcell themselves investigated the precision of a single receptor that binds and unbinds molecules [5]. For a receptor with lengthscale s, they found, again using the autocorrelation function, a relative error of

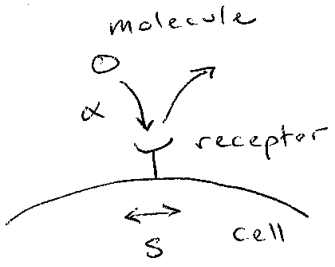

Figure 4: Receptor binding.

$$\epsilon^2 = \frac{1}{2(1-p)}\frac{1}{sTc_0D}, \tag{26}$$

where p is the probability that the receptor is bound. Notice that error diverges in the limit $p \to 1$, because then the receptor is saturated and can detect no new molecules.

In 2005, Bialek and Setayeshgar generalized the problem to account for the fluctuations in the binding and unbinding kinetics of the receptor itself [8]. Using the fluctuation-dissipation theorem, they found

$$\epsilon^2 = \frac{1}{\pi}\frac{1}{sTc_0D} + \frac{2}{(1-p)kc_0T}, \tag{27}$$

where k is the binding rate. In 2014, Kaizu et al. improved upon this calculation to properly account for diffusive rebinding events [9]. Using reaction-diffusion theory, they found

$$\epsilon^2 = \frac{1}{2\pi(1-p)}\frac{1}{sTc_0D} + \frac{2}{(1-p)kc_0T}. \tag{28}$$

In Eqs. 27 and 28, the second term comes from the additional noise of binding and unbinding. Importantly, however, in all of Eqs. 26-28, there is a term that scales as Eq. 1. The prefactor or additional terms may depend on the model, but the limit given by Berg and Purcell in Eq. 1 always sets the maximal precision.

2.4 Do actual cells approach the limit?

After deriving the limit to the precision of concentration sensing, Berg and Purcell then asked whether actual cells were observed to reach this limit [5]. They focused on data from several types of single-celled organisms, including the *Escheria coli* bacterium. Motility of *E. coli* has two distinct phases: the "run" phase in which a cell swims in a fixed direction, and the "tumble" phase in which the cell randomly rotates in order to begin a new run in a different direction (**Fig. 5**). The bacterium biases its motion toward higher chemical concentrations by continually measuring the concentration and extending the time of runs for which the change in concentration is positive. The change in concentration over a run time T depends on the concentration gradient $g = \partial c/\partial x$ and the bacterium's velocity v,

$$\Delta c = Tgv. \tag{29}$$

Berg and Purcell argued that for a change in concentration to be detectable, it must be larger than the measurement error, $\Delta c > \sigma_c$. Using for the relative error the scaling in Eq. 1,

$$\frac{\sigma_c^2}{c_0^2} \sim \frac{1}{aTc_0D}, \qquad (30)$$

we obtain a lower limit on the run time,

$$T_{\min} \sim \left[\frac{c_0}{aDv^2g^2}\right]^{1/3}. \qquad (31)$$

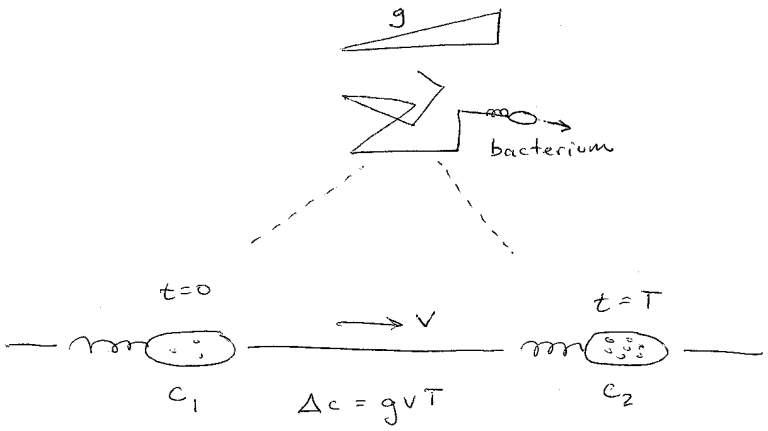

Figure 5: Run-and-tumble chemotaxis.

Typical values for the sensory threshold of *E. coli* are on the order of $c_0 = 1$ mM, $g = 10$ nM/μm, $a = 1$ μm, $v = 10$ μm/s, and $D = 10^3$ μm^2/s [5]. Using the fact that one nanomolar is about one molecule per cubic micron, Eq. 31 evaluates to

$$T_{\min} \sim \left[\left(\frac{10^6 \text{ nM}}{1}\right)\left(\frac{1}{1\ \mu\text{m}}\right)\left(\frac{1 \text{ s}}{10^3\ \mu\text{m}^2}\right)\left(\frac{1 \text{ s}}{10\ \mu\text{m}}\right)^2\left(\frac{1\ \mu\text{m}}{10 \text{ nM}}\right)^2\left(\frac{1 \text{ nM}}{1\ \mu\text{m}^{-3}}\right)\right]^{1/3} = 0.5 \text{ s}. \qquad (32)$$

Actual run times are on the order of $T_{\text{obs}} \sim 1$ s. The fact that $T_{\text{obs}} > T_{\min}$ implies that the observed sensory behavior of *E. coli* is consistent with the physical bound. However, the fact that T_{obs} is also *very close* to $T_{\min}$ implies, as Berg and Purcell concluded, that the design of the sensory machinery in *E. coli* is nearly optimal. If the run times were much shorter, gradient tracking would be physically impossible.

3 Limits to multicellular sensing

No cell is an island. Cells exist in complex communities, and within these communities they communicate. Can communication enhance the precision of sensing? Here I will present some recent experiments investigating this question, and theoretical work by my group to extend the considerations above to communicating cell populations.

3.1 Evidence for collective sensing

In a developing fruit fly embryo, cell nuclei determine their fate by detecting molecules called morphogens, whose concentration varies from one end of the embryo to the other (**Fig. 6**). In one well-studied case [10], the concentration of a morphogen called Bicoid decays exponentially with lengthscale $\Lambda \approx 100$ μm. Nuclei that detect a Bicoid concentration above a threshold of $c_0 \approx 5$ μm^{-3} express a particular gene, and the other nuclei do not. Because nuclei are $a \approx 8$ μm wide, this means that nuclei near the expression boundary detect the Bicoid concentration with a precision of $a/\Lambda \approx 10\%$.

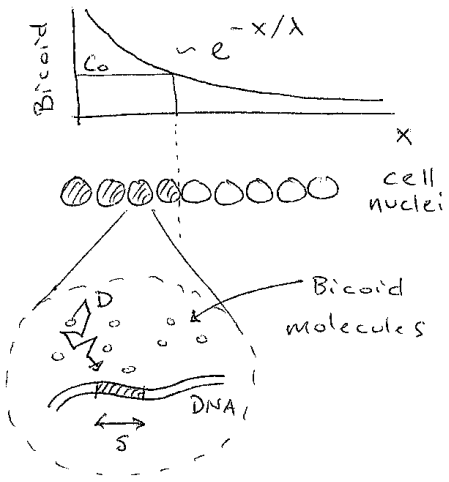

Figure 6: Embryonic development.

How long would it take to achieve this precision? Bicoid has a diffusion coefficient in the embryo of $D \approx 1$ μm^2/s, and it is detected by a binding site along the nuclear DNA with lengthscale $s \approx 3$ nm. Therefore, according to the Berg-Purcell scaling (Eq. 1), a precision of $\epsilon = 10\%$ would require

$$T \sim \frac{1}{sc_0 D\epsilon^2} = \left(\frac{1}{3\times 10^{-3}\ \mu\text{m}}\right)\left(\frac{1}{5\ \mu\text{m}^{-3}}\right)\left(\frac{1\text{ s}}{1\ \mu\text{m}^2}\right)\left(\frac{1}{10^{-1}}\right)^2 = 7\times 10^3\text{ s}, \tag{33}$$

or almost 2 hours. The problem is that at this point the embryo has only existed for about two hours, and the nuclei in their present locations have only just formed toward the end of this time period, during the latest division cycle. Therefore it is likely that the nuclei perform their detection in a far shorter time period. But then how do they achieve the necessary precision?

A possible answer, proposed by Gregor et al. [10] and later explored in more detail [11], is that the nuclei communicate, e.g. by diffusively exchanging a messenger molecule. In principle, this communication could allow nuclei to share measurement information and therefore achieve a desired precision within a time that is less than if each nucleus relied only on its own measurements.

Indeed, more recent work has explicitly demonstrated that cell-cell communication improves the precision of sensing. Epithelial cells can detect concentration gradients of 50 nM/mm but cannot detect gradients one hundred times shallower [12]. However, groups of epithelial cells *can* detect the shallower gradients. Importantly, when the gap junctions between these cells (portals that allow molecules to be exchanged across cell membranes) are blocked with a drug, this detection ability vanishes [12]. This result demonstrates explicitly that cells can use gap-junction communication to improve sensory precision.

3.2 Sensing with short-range communication

To explore theoretically how communication can improve the precision of concentration sensing, we consider two ubiquitous types of cell-cell communication [13]. The first is short-range communication (also called juxtacrine signaling), where cells pass molecules directly across their membranes, e.g. via gap junctions (**Fig. 7**). We consider the simplest case of two adjacent cells with radii a. As before we assume that the cells are sensing a uniform concentration with average value c_0. Molecules bind to receptors on each cell's surface, leading to bound receptor numbers r_1 and r_2. Bound receptors produce messenger molecules, leading to m_1 and m_2 molecules in each cell, respectively, and these are exchanged between cells at a rate γ to provide the communication. The dynamics of the concentration, bound receptor numbers, and messenger molecule numbers are

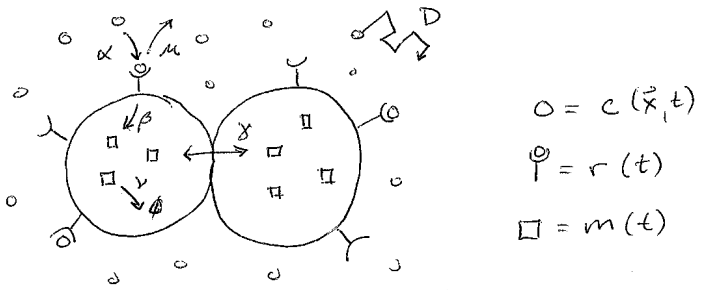

Figure 7: Sensing with short-range communication.

$$\dot{c} = D\nabla^2 c - \delta(\vec{x}-\vec{x}_1)\dot{r}_1 - \delta(\vec{x}-\vec{x}_2)\dot{r}_2 + \eta, \tag{34}$$

$$\dot{r}_{1,2} = \alpha c(\vec{x}_{1,2}, t) - \mu r_{1,2} + \xi_{1,2}, \tag{35}$$

$$\dot{m}_{1,2} = \beta r_{1,2} - \nu m_{1,2} + \gamma(m_{2,1} - m_{1,2}) + \chi_{1,2}, \tag{36}$$

where $|\vec{x}_2 - \vec{x}_1| = 2a$ is the cell separation; α and μ are the receptor binding and unbinding rates, respectively; and β and ν are the messenger production and degradation rates, respectively. Eq. 34 treats each cell as a point, but the cell radius a can be reintroduced later in the Fourier analysis as a small-wavelength cutoff [8, 13]. Eq. 35 neglects the effects of receptor saturation.

As before, Eqs. 34-36 include Langevin noise terms η, ξ_i, and χ_i to account for the fluctuations in diffusion; the binding and unbinding reactions; and the production, degradation, and exchange reactions, respectively. Their statistics are

$$\langle \eta(\vec{x}', t')\eta(\vec{x}, t)\rangle = 2Dc_0\delta(t-t')\vec{\nabla}_x \cdot \vec{\nabla}_{x'}\delta(\vec{x}-\vec{x}'), \tag{37}$$

$$\langle \xi_i(t)\xi_j(t')\rangle = 2\mu\bar{r}\delta(t-t')\delta_{ij}, \tag{38}$$

$$\langle \chi_i(t)\chi_j(t')\rangle = 2\bar{m}\delta(t-t')\left[(\nu+\gamma)\delta_{ij} - \gamma(1-\delta_{ij})\right]. \tag{39}$$

Eq. 37 is the same as before (Eq. 21), while Eqs. 38 and 39 are proportional to the associated reaction propensities [14]. Here, $\bar{r} = \alpha c_0/\mu$ and $\bar{m} = \beta\bar{r}/\nu$ are the mean numbers of bound receptors and messenger molecules in each cell, respectively. Note that the last term in Eq. 39 accounts for the anti-correlations associated with messenger exchange. That is, communication is equivalent to diffusive hopping on a lattice, and here the lattice has only two sites (the cells). Therefore, as above, the loss of a molecule in one cell produces a gain of one molecule in the neighboring cell, leading to anti-correlations.

Eqs. 34-36 constitute a linear system, and therefore the power spectra can be calculated in the same way as in Sec. 2.2 [13]. This allows one to obtain the relative error in the time-average of the messenger molecule number in either cell. The result is

$$\epsilon^2 = \frac{\sigma_T^2}{\bar{m}^2} = \left[\frac{\nu^2+3\nu\gamma+3\gamma^2}{2\pi(\nu+2\gamma)^2}\right]\frac{1}{aTc_0D} + \left[\frac{2(\nu^2+2\nu\gamma+2\gamma^2)}{(\nu+2\gamma)^2}\right]\frac{1}{\mu T\bar{r}} + \left[\frac{2(\nu+\gamma)}{\nu+2\gamma}\right]\frac{1}{\nu T\bar{m}}. \tag{40}$$

The first term is the Berg-Purcell limit, where now the prefactor depends on the communication via the ratio of the exchange rate γ to the degradation rate ν of the messenger molecule. The last two terms come from fluctuations in the bound receptor number and the messenger molecule number, respectively. They scale inversely with the means, $\bar{r}$ and $\bar{m}$, as we would expect for Poisson statistics. They also scale inversely with the numbers of independent measurements μT and νT that can be made in the time T given their turnover rates, respectively. These last two terms can always be made small by the cell increasing the number or turnover of its molecules, but the first term depends on the environment and is therefore unavoidable. We focus only on the first term from here on.

In the limits of weak and strong communication, the first term of Eq. 40 becomes

$$\epsilon^2 = \frac{1}{\pi aTc_0D} \times \begin{cases} 1/2 & \gamma \ll \nu \\ 3/8 & \gamma \gg \nu. \end{cases} \tag{41}$$

The top case is equivalent to the single-cell limit in this model, because in this case the cells are not communicating. The bottom case is the perfect-communication limit for the two cells. Surprisingly, because 3/8 is more than half of 1/2, we see that doubling the cell number has not halved the error, even for perfect communication. Why not?

The reason is that the cells are adjacent to each other and are therefore sampling adjacent portions of the environment. As a result, the molecules counted by the two cells are not independent, and we do not get the error reduction we expect for independent variables.

In fact, this model can be generalized to N cells arranged in a sphere (**Fig. 8**, left) [13], and the relative error also does not fall off like $1/N$. Instead, it falls off less steeply due to the environmental cross-correlations between cells, like $\epsilon^2 \sim 1/N^{1/3}$ (**Fig. 9**, left). We can understand this scaling immediately: the volume of the N-cell cluster scales like Na^3, and therefore its length scales like $N^{1/3}a$. Thus, its relative error should obey the Berg-Purcell limit, but with $N^{1/3}a$ in place of a, namely $\epsilon^2 \sim 1/(N^{1/3}aTc_0D)$, as indeed observed.

3.3 Sensing with long-range communication

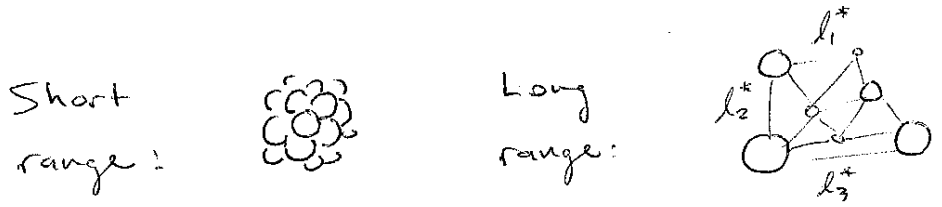

Figure 8: Many cells.

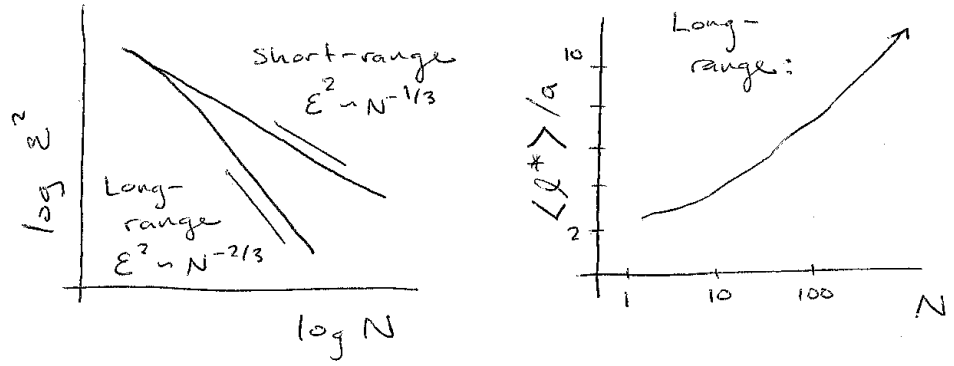

Figure 9: Relative error and nearest-neighbor cell separation.

The second type of communication that we explore is long-range communication (also called autocrine signaling), where cells secrete the messenger molecules into the environment, and the molecules diffuse and are detected by other cells or the same cell (**Fig. 10**) [13]. In this case the cells need not be (and often are not) adjacent. Therefore we may expect some alleviation of the environmental cross-correlations suffered by cells using short-range communication, although we also expect that if cells get too far apart they lose the ability to communicate altogether.

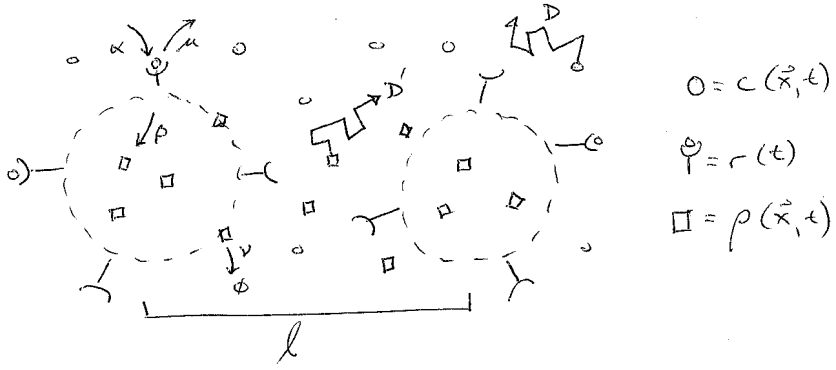

Figure 10: Sensing with long-range communication.

Again we consider the simplest case of two cells, this time separated by a distance ℓ. Because the diffusion and binding of signal molecules to cell receptors remains the same as in the previous case, Eqs. 34 and 35 still hold here. However, Eq. 36 is replaced by a secretion-and-diffusion equation for the messenger molecules,

$$\dot{\rho} = D'\nabla^2\rho - \nu\rho + \delta(\vec{x} - \vec{x}_1)(\beta r_1 + \zeta_1) + \delta(\vec{x} - \vec{x}_2)(\beta r_2 + \zeta_2) + \psi, \tag{42}$$

Here $\rho(\vec{x}, t)$ is the messenger molecule concentration and D' is the messenger molecule diffusion coefficient.

The noise terms obey [7, 14]

$$\langle \zeta_i(t)\zeta_j(t')\rangle = \beta\bar{r}\delta(t - t')\delta_{ij}, \tag{43}$$

$$\langle \psi(\vec{x}, t)\psi(\vec{x}', t')\rangle = \nu\bar{\rho}(\vec{x})\delta(t - t')\delta(\vec{x} - \vec{x}') + 2D'\delta(t - t')\vec{\nabla}_x \cdot \vec{\nabla}_{x'} \left[\bar{\rho}(\vec{x})\delta(\vec{x} - \vec{x}')\right], \tag{44}$$

where

$$\bar{\rho}\left(\vec{x}\right) = \frac{\beta\bar{r}}{4\pi D'}\left(\frac{e^{-|\vec{x}-\vec{x}_1|/\lambda}}{|\vec{x}-\vec{x}_1|} + \frac{e^{-|\vec{x}-\vec{x}_2|/\lambda}}{|\vec{x}-\vec{x}_2|}\right) \tag{45}$$

is the average concentration profile of the messenger molecules in steady state, and the lengthscale of communication is set by $\lambda \equiv \sqrt{D'/\nu}$. Eq. 45 illustrates that indeed the strength of communication falls off with the distance from each source. Even in the perfect-communication limit ($\lambda \to \infty$), in which the exponential terms in Eq. 45 go to unity, there is still a power-law falloff due to the inability of diffusion to fill 3D space.

To detect the messenger molecules, we imagine, as with the perfect instrument (Sec. 2.2), that each cell is permeable to them and counts the number in its volume V_i,

$$m_i(t) = \int_{V_i} d^3x \rho(\vec{x}, t). \tag{46}$$

Once again, the power spectra can be calculated to obtain the relative error in the average of m over a time T [13]. Keeping only the Berg-Purcell term and taking the perfect-communication limit $\lambda \to \infty$, the result is

$$\epsilon^2 = \frac{\sigma_T^2}{\bar{m}^2} = \left[\frac{16a^2 + 9\ell^2}{2\pi(2a+3\ell)^2}\right]\frac{1}{aTc_0D}. \tag{47}$$

Eq. 47 has the following limits,

$$\epsilon^2 = \frac{1}{\pi aTc_0D} \times \begin{cases} 1/2 & \ell \gg a \\ 2/5 & \ell = \ell^* = 8a/3. \end{cases} \tag{48}$$

The top case corresponds to large cell separation. Here we expect communication not to play a role, and indeed we recover the single-cell limit of Eq. 41 (top case). The bottom case reflects the fact that Eq. 47 has a minimum as a function of ℓ. The minimum comes from the anticipated tradeoff: at large ℓ the communication is too weak, but at small ℓ the cells are sampling adjacent regions of the environment leading to cross-correlations in their measurements. The minimum occurs at $\ell^* = 8a/3 \approx 2.7a$, slightly more than a diameter apart.

The optimal precision for two cells is similar for both short- and long-range communication ($3/8 = 0.375$ is close to $2/5 = 0.4$). This makes sense because the optimal separation in the long-range case is not much more than a diameter. However, the situation changes as the number of cells N grows. Using numerical optimization, it is straightforward to find the optimal cell positions in the long-range case for any N (**Fig. 8**, right) [13]. The resulting relative error then falls off more steeply than $N^{-1/3}$ (**Fig. 9**, left). Indeed, after our work was published, a different group proved that the scaling is $N^{-2/3}$ [15]. Evidently, long-range communication allows higher sensory precision than short-range communication for large cell populations.

Even more striking is that the average optimal separation $\langle \ell^* \rangle$ between nearest-neighbors in the long-range case grows with N (**Fig. 9**, right). With a few hundred cells, nearest neighbors are separated by about five cell diameters. This highlights the statistical advantage of spreading out in order to sample a larger portion of the environment. Indeed, it is known that some tumor cells that communicate by autocrine signaling actively spread themselves out by several cell diameters, and it has been shown that this strategy minimizes fluctuations in the signals they detect [16].

4 Concluding remarks

The legacy of Berg and Purcell is long and continues to grow. Their original insights on the physical limits to chemical sensing [5] have been refined [8, 9, 17] and extended to communicating cell populations [13], to spatial gradient sensing by single cells [6, 18, 19, 20] and populations [21, 22], to temporal gradient

sensing [23], to simultaneous sensing of multiple molecule types [24], and to sensing in different confinement geometries [25]. These theoretical limits have been put to the test in bacteria [5, 8], amoebae [6], fruit flies [10], epithelia [12], neurons [26], our immune system [24], and tumors [13], and in most cases one finds that cells have evolved to approach the limits closely. Precise sensing is critical for cell survival, and evidently cells will do everything physically possible to achieve it.

A Integral evaluations

The derivation of Eq. 15 proceeds as

$$\tilde{\delta n}(\omega) = \int dt\ \delta n(t) e^{i\omega t} \tag{49}$$

$$= \int dt \int_V d^3x\ \delta c(\vec{x},t) e^{i\omega t} \tag{50}$$

$$= \int dt \int_V d^3x \int \frac{d^3k}{(2\pi)^3}\frac{d\omega'}{2\pi}\ \tilde{\delta c}(\vec{k},\omega') e^{-i\vec{k}\cdot\vec{x}-i\omega' t} e^{i\omega t} \tag{51}$$

$$= \int_V d^3x \int \frac{d^3k}{(2\pi)^3}\ \tilde{\delta c}(\vec{k},\omega) e^{-i\vec{k}\cdot\vec{x}}. \tag{52}$$

where the first line is the definition of the Fourier transform, the second line follows from Eq. 11, the third line inserts the inverse Fourier transform for $\delta c(\vec{x},t)$, and the last line employs the relation $\int dt\ e^{i(\omega-\omega')t} = 2\pi\delta(\omega-\omega')$ to evaluate the t integral and then collapse the ω' integral.

The evaluation of Eq. 23,

$$S_n(0) = \frac{2c_0}{D}\int_V d^3x d^3x' \int \frac{d^3k}{(2\pi)^3}\ \frac{e^{-i\vec{k}\cdot(\vec{x}-\vec{x}')}}{k^2}, \tag{53}$$

proceeds as follows. We separate the $\vec{x}$ and $\vec{x}'$ integrals into their radial and angular components,

$$S_n(0) = \frac{2c_0}{D}\int \frac{d^3k}{(2\pi)^3}\ \frac{1}{k^2}\int_0^a dx\ x^2 \int d\Omega_x\ e^{-i\vec{k}\cdot\vec{x}} \int_0^a dx'\ x'^2 \int d\Omega_{x'}\ e^{i\vec{k}\cdot\vec{x}'}. \tag{54}$$

Then we use the expansion of the plane wave in spherical Bessel functions and spherical harmonics to evaluate the solid angle integrals,

$$\int d\Omega_x\ e^{\pm i\vec{k}\cdot\vec{x}} = \int d\Omega_x \sum_{\ell=0}^{\infty}\sum_{m=-\ell}^{\ell} j_\ell(\pm kx) Y^*_{\ell m}(\pm\hat{k}) Y_{\ell m}(\hat{x}) \tag{55}$$

$$= \sum_{\ell=0}^{\infty}\sum_{m=-\ell}^{\ell} j_\ell(\pm kx) Y^*_{\ell m}(\pm\hat{k}) \int d\Omega_x\ \sqrt{4\pi} Y^*_{00}(\hat{x}) Y_{\ell m}(\hat{x}) \tag{56}$$

$$= \sum_{\ell=0}^{\infty}\sum_{m=-\ell}^{\ell} j_\ell(\pm kx) Y^*_{\ell m}(\pm\hat{k}) \sqrt{4\pi}\delta_{\ell 0}\delta_{m0} \tag{57}$$

$$= j_0(\pm kx) Y^*_{00}(\pm\hat{k})\sqrt{4\pi} \tag{58}$$

$$= 4\pi j_0(kx), \tag{59}$$

where the second line uses the fact that $Y_{00} = 1/\sqrt{4\pi}$, the third and fourth lines use the orthonormality of the spherical harmonics to evaluate the integral and collapse the sums, and the fifth line uses the fact that

$j_0(u) = (\sin u)/u$ is even. Applying Eq. 59 to Eq. 54 we obtain

$$S_n(0) = \frac{2c_0}{D} \int \frac{d^3k}{(2\pi)^3} \frac{1}{k^2} \left[\int_0^a dx\ x^2 \times 4\pi j_0(kx) \right]^2 \tag{60}$$

$$= \frac{16c_0}{D} \int_0^\infty \frac{dk}{k^6} \left[\int_0^{ka} du\ u^2 j_0(u) \right]^2, \tag{61}$$

where the second step separates the $\vec{k}$ integral into its radial and angular components and defines $u = kx$. Now we make use of the following two properties of spherical Bessel functions,

$$\int du\ u^2 j_0(u) = u^2 j_1(u), \tag{62}$$

$$\int_0^\infty du\ u^{v-1} j_w^2(u) = \frac{\sqrt{\pi}}{2(1-v)} \frac{\Gamma[1-(v/2)]\Gamma[(v/2)+w]}{\Gamma[(1-v)/2]\Gamma[2-(v/2)+w]} \qquad (-2w < v < 2), \tag{63}$$

where Γ is the Gamma function. The first property can be verified using integration by parts and the fact that $j_1(u) = (\sin u - u\cos u)/u^2$. We apply the first property to Eq. 61 to obtain

$$S_n(0) = \frac{16c_0a^5}{D} \int_0^\infty \frac{du}{u^2}\ j_1^2(u), \tag{64}$$

where now $u = ka$. We apply the second property with $v = -1$ and $w = 1$ to Eq. 64 to obtain

$$S_n(0) = \frac{16\pi c_0 a^5}{15D}. \tag{65}$$

as in Eq. 24, where we have used the facts that $\Gamma(1/2) = \sqrt{\pi}$, $\Gamma(1) = 1$, $\Gamma(3/2) = \sqrt{\pi}/2$, and $\Gamma(7/2) = 15\sqrt{\pi}/8$.

B Variance and the power spectrum

Here we show that the variance in the long-time average of a variable is given by the low-frequency limit of its power spectrum.

First we show that the power spectrum and autocorrelation function are related by Fourier transform, since we will use that result in the derivation. For a variable $x(t)$ with zero mean, the power function reads

$$S(\omega) = \int \frac{d\omega'}{2\pi} \langle \tilde{x}^*(\omega')\tilde{x}(\omega) \rangle \tag{66}$$

$$= \int \frac{d\omega'}{2\pi} dt dt'\ \langle x(t')x(t) \rangle\, e^{i\omega t} e^{-i\omega' t'}, \tag{67}$$

where the second step inserts the Fourier transforms. The quantity $C(t-t') = \langle x(t')x(t) \rangle$ is the autocorrelation function. The ω' integral evaluates to a delta function, which collapses the t' integral,

$$S(\omega) = \int dt dt'\ C(t-t') e^{i\omega t} \delta(t') \tag{68}$$

$$= \int dt\ C(t) e^{i\omega t}. \tag{69}$$

We see that the power spectrum is the Fourier transform of the autocorrelation function. Therefore

$$C(t) = \int \frac{d\omega}{2\pi} S(\omega) e^{-i\omega t} \tag{70}$$

is the inverse transform.

Now consider the variance in the time-average of $x(t)$ over a time T,

$$\sigma_T^2 = \left\langle \frac{1}{T}\int_0^T dt\ x(t) \times \frac{1}{T}\int_0^T dt'\ x(t') \right\rangle \tag{71}$$

$$= \frac{1}{T^2}\int_0^T dtdt'\ \langle x(t)x(t')\rangle \tag{72}$$

$$= \frac{1}{T^2}\int_0^T dtdt'\ C(t-t'). \tag{73}$$

We transform variables as $\tau = t - t'$ and $\tau' = t + t'$. Eq. 73 becomes

$$\sigma_T^2 = \frac{1}{2T^2}\int_{-T}^T d\tau \int_{|\tau|}^{2T-|\tau|} d\tau'\ C(\tau) \tag{74}$$

where the extra factor of $1/2$ comes from the Jacobian. This allows us to perform the τ' integration,

$$\sigma_T^2 = \frac{1}{T^2}\int_{-T}^T d\tau\ (T-|\tau|)C(\tau). \tag{75}$$

We insert Eq. 70,

$$\sigma_T^2 = \frac{1}{T^2}\int_{-T}^T d\tau\ (T-|\tau|)\int \frac{d\omega}{2\pi}S(\omega)e^{-i\omega\tau}, \tag{76}$$

and perform the τ integration by breaking up the integral,

$$\sigma_T^2 = \frac{1}{T^2}\int \frac{d\omega}{2\pi}S(\omega)\left[\int_{-T}^0 d\tau\ (T+\tau)e^{-i\omega\tau} + \int_0^T d\tau\ (T-\tau)e^{-i\omega\tau}\right] \tag{77}$$

$$= \frac{1}{T^2}\int \frac{d\omega}{2\pi}S(\omega)\left[\int_0^T d\tau\ (T-\tau)e^{i\omega\tau} + \int_0^T d\tau\ (T-\tau)e^{-i\omega\tau}\right] \tag{78}$$

$$= \frac{2}{T^2}\int \frac{d\omega}{2\pi}S(\omega)\int_0^T d\tau\ (T-\tau)\cos(\omega\tau) \tag{79}$$

$$= \frac{2}{T^2}\int \frac{d\omega}{2\pi}S(\omega)\frac{1-\cos(\omega T)}{\omega^2} \tag{80}$$

$$= \frac{4}{T^2}\int \frac{d\omega}{2\pi}S(\omega)\frac{\sin^2(\omega T/2)}{\omega^2} \tag{81}$$

$$= \frac{1}{\pi T}\int_{-\infty}^{\infty} du\ S(2u/T)j_0^2(u). \tag{82}$$

Here the second line takes $\tau \to -\tau$ in the first integral in the brackets; the third line uses $e^{-i\omega\tau} + e^{-i\omega\tau} = 2\cos(\omega\tau)$; the fourth line uses integration by parts; the fifth line uses the trigonometric identity $1 - \cos\theta = 2\sin^2(\theta/2)$; and the sixth line defines $u = \omega T/2$, recalls that $j_0(u) = (\sin u)/u$, and makes explicit the infinite range of integration.

In the limit of large T we can take $S(2u/T) \to S(0)$ and remove it from the integral. More precisely, this action is valid when $S(\omega)$ is roughly constant for $|\omega| \lesssim T^{-1}$ because the presence of $j_0^2(u)$ in Eq. 82 gives the integral support only when $|u|$ is order one. In general the power spectrum is constant below the lowest characteristic frequency of the system, or equivalently the inverse of the longest characteristic timescale. Thus, we must have T longer than the longest characteristic timescale of the system to take

$S(2u/T) \to S(0)$. Assuming this is true, Eq. 82 becomes

$$\sigma_T^2 = \frac{S(0)}{\pi T} \int_{-\infty}^{\infty} du\ j_0^2(u) \tag{83}$$

$$= \frac{S(0)}{T}, \tag{84}$$

as in Eq. 16. The second step uses the following property of spherical Bessel functions,

$$\int_0^{\infty} du\ j_v^2(u) = \frac{\pi}{4v+2} \qquad (v > -1/2), \tag{85}$$

with $v = 0$, and the fact that $j_0^2(u)$ is even. We see in Eq. 84 that the variance in the long-time average of a variable is the low-frequency limit of its power spectrum divided by the averaging time.

References

[1] Foster Rieke and Denis A Baylor. Single-photon detection by rod cells of the retina. *Reviews of Modern Physics*, 70(3):1027, 1998.

[2] Jürgen Boeckh, Karl-Ernst Kaissling, and Dietrich Schneider. Insect olfactory receptors. In *Cold Spring Harbor Symposia on Quantitative Biology*, volume 30, pages 263–280. Cold Spring Harbor Laboratory Press, 1965.

[3] Jun Huang, Mario Brameshuber, Xun Zeng, Jianming Xie, Qi-jing Li, Yueh-hsiu Chien, Salvatore Valitutti, and Mark M Davis. A single peptide-major histocompatibility complex ligand triggers digital cytokine secretion in CD4+ T cells. *Immunity*, 39(5):846–857, 2013.

[4] Loling Song, Sharvari M Nadkarni, Hendrik U Bödeker, Carsten Beta, Albert Bae, Carl Franck, Wouter-Jan Rappel, William F Loomis, and Eberhard Bodenschatz. Dictyostelium discoideum chemotaxis: threshold for directed motion. *European Journal of Cell Biology*, 85(9-10):981–989, 2006.

[5] Howard C Berg and Edward M Purcell. Physics of chemoreception. *Biophysical Journal*, 20(2):193–219, 1977.

[6] Robert G Endres and Ned S Wingreen. Accuracy of direct gradient sensing by single cells. *Proceedings of the National Academy of Sciences*, 2008.

[7] Crispin W Gardiner. *Handbook of stochastic methods for physics, chemistry, and the natural sciences*. Springer-Verlag Berlin, 3rd edition, 2004.

[8] William Bialek and Sima Setayeshgar. Physical limits to biochemical signaling. *Proceedings of the National Academy of Sciences*, 102(29):10040–10045, 2005.

[9] Kazunari Kaizu, Wiet de Ronde, Joris Paijmans, Koichi Takahashi, Filipe Tostevin, and Pieter Rein ten Wolde. The Berg-Purcell limit revisited. *Biophysical Journal*, 106(4):976–985, 2014.

[10] Thomas Gregor, David W Tank, Eric F Wieschaus, and William Bialek. Probing the limits to positional information. *Cell*, 130(1):153–164, 2007.

[11] Thorsten Erdmann, Martin Howard, and Pieter Rein ten Wolde. Role of spatial averaging in the precision of gene expression patterns. *Physical Review Letters*, 103(25):258101, 2009.

[12] David Ellison, Andrew Mugler, Matthew D Brennan, Sung Hoon Lee, Robert J Huebner, Eliah R Shamir, Laura A Woo, Joseph Kim, Patrick Amar, Ilya Nemenman, Andrew J Ewald, and Andre Levchenko. Cell–cell communication enhances the capacity of cell ensembles to sense shallow gradients during morphogenesis. *Proceedings of the National Academy of Sciences*, 113(6):E679–E688, 2016.

[13] Sean Fancher and Andrew Mugler. Fundamental limits to collective concentration sensing in cell populations. *Physical Review Letters*, 118(7):078101, 2017.

[14] Daniel T Gillespie. The chemical Langevin equation. *The Journal of Chemical Physics*, 113(1):297–306, 2000.

[15] David B Saakian. Kinetics of biochemical sensing by single cells and populations of cells. *Physical Review E*, 96(4):042413, 2017.

[16] Nataly Kravchenko-Balasha, Jun Wang, Francoise Remacle, RD Levine, and James R Heath. Glioblastoma cellular architectures are predicted through the characterization of two-cell interactions. *Proceedings of the National Academy of Sciences*, 111(17):6521–6526, 2014.

[17] Robert G Endres and Ned S Wingreen. Maximum likelihood and the single receptor. *Physical Review Letters*, 103(15):158101, 2009.

[18] Geoffrey J Goodhill and Jeffrey S Urbach. Theoretical analysis of gradient detection by growth cones. *Journal of Neurobiology*, 41(2):230–241, 1999.

[19] Robert G Endres and Ned S Wingreen. Accuracy of direct gradient sensing by cell-surface receptors. *Progress in Biophysics and Molecular Biology*, 100(1-3):33–39, 2009.

[20] Bo Hu, Wen Chen, Wouter-Jan Rappel, and Herbert Levine. Physical limits on cellular sensing of spatial gradients. *Physical Review Letters*, 105(4):048104, 2010.

[21] Andrew Mugler, Andre Levchenko, and Ilya Nemenman. Limits to the precision of gradient sensing with spatial communication and temporal integration. *Proceedings of the National Academy of Sciences*, 113(6):E689–E695, 2016.

[22] Julien Varennes, Sean Fancher, Bumsoo Han, and Andrew Mugler. Emergent versus individual-based multicellular chemotaxis. *Physical Review Letters*, 119(18):188101, 2017.

[23] Thierry Mora and Ned S Wingreen. Limits of sensing temporal concentration changes by single cells. *Physical Review Letters*, 104(24):248101, 2010.

[24] Thierry Mora. Physical limit to concentration sensing amid spurious ligands. *Physical Review Letters*, 115(3):038102, 2015.

[25] Brendan A Bicknell, Peter Dayan, and Geoffrey J Goodhill. The limits of chemosensation vary across dimensions. *Nature Communications*, 6:7468, 2015.

[26] William J Rosoff, Jeffrey S Urbach, Mark A Esrick, Ryan G McAllister, Linda J Richards, and Geoffrey J Goodhill. A new chemotaxis assay shows the extreme sensitivity of axons to molecular gradients. *Nature Neuroscience*, 7(6):678, 2004.